PHYSICAL REVIEW D **89,** 023007 (2014)

Isospin dependence of entrainment in superfluid neutron stars in a relativistic model

Apurba Kheto and Debades Bandyopadhyay

Astroparticle Physics and Cosmology Division and Centre for Astroparticle Physics, Saha Institute of Nuclear Physics, 1/AF Bidhannagar, Kolkata-700064, India

(Received 27 August 2013; published 14 January 2014)

We study the entrainment effect between superfluid neutrons and charge neutral fluid (called the proton fluid) which is made of protons and electrons in a neutron star interior within the two-fluid formalism and using a relativistic model where baryon-baryon interaction is mediated by the exchange of σ, ω, and ρ mesons. This model of strong interaction also includes scalar self-interactions. The entrainment matrix and entrainment parameter are calculated using the parameter sets of Glendenning (GL) and another non-linear (NL3) interaction. The inclusion of ρ mesons strongly influences the entrainment parameter ($\varepsilon_{\rm mom}$) in a superfluid neutron star. The entrainment parameter is constant at the core and drops rapidly at the surface. It takes values within the physical range.

DOI: 10.1103/PhysRevD.89.023007 PACS numbers: 97.60.Jd, 47.75.+f, 95.30.Sf

I. INTRODUCTION

Novel phases of dense matter might exist in neutron stars. Superfluidity or superconductivity is one such form of matter. Recently, rapid cooling of the neutron star in Cassiopeia A was reported [1]. This has been attributed to the neutron superfluidity in neutron star cores [2]. Pulsar glitches are also thought to be the manifestation of superfluidity in the crust and core of neutron stars [3–6]. This glitch phenomenon might be described based on the pinning and unpinning of superfluid quantized vortices in neutron stars.

Superfluidity in neutron stars was studied in great detail in Newtonian and general relativistic formulations [7–9]. The fluid formalism in the case of superfluidity is different from that of the perfect fluid. For neutron stars made of neutrons, protons, and electrons, two-fluid formalism was used to describe the superfluidity in neutron star matter [8]. In this case, one fluid is the superfluid neutrons and the other fluid, called the proton fluid, represents the charge neutral component made of protons and electrons. It is a well-known fact that two fluids in a mixture are not decoupled when one fluid interpenetrates through the other. In this situation, the momentum of one fluid is proportional to the linear combination of the velocities of both fluids. This effect is known as entrainment. The entrainment effect has been studied intensively in understanding rotational equilibria, oscillations of superfluid neutron stars [7,10–13], and the pulsar glitch [5,6].

Superfluid dynamics including entrainment in neutron stars were studied using Newtonian calculations. The entrainment effect in nonrelativistic and relativistic Fermi-liquid models was studied by different groups [14–17]. A similar model was developed for entrainment to study slowly rotating superfluid Newtonian neutron stars [7]. Comer and Joynt calculated the entrainment effect in a relativistic field theoretical model and obtained first order corrections to the slowly rotating superfluid neutron stars [18] for the first time. However, the relativistic model was inadequate to describe the neutron star matter because the σ-ω Walecka model was adopted in this calculation. Neutron star matter is highly asymmetric and the inclusion of ρ mesons in the Walecka model is absolutely necessary. Consequently, it is worth studying the effects of symmetry energy on the master function and superfluid dynamics in neutron stars. This motivates us to extend the calculation of Comer and Joynt [18,19] to include ρ mesons along with scalar self-interactions.

We organize the paper in the following way. We describe the relativistic σ-ω-ρ model for entrainment and the connection between the master function and relativistic mean field model, as well as the formalism for slowly rotating superfluid neutron stars, in Sec. II. Results of this calculation are discussed in Sec. III. Section IV gives the summary and conclusions.

II. FORMALISM

Here we adopt the two-fluid formalism as described in Refs. [20–27] to study the entrainment effect in cold neutron stars. The signature of the metric used here is the same as in Ref. [18]. The starting point of the superfluid formalism is the master function (Λ). It is a function of scalars which are constructed from neutron (n^μ) and proton (p^μ) number density currents such as $n^2 = -n_\mu n^\mu$, $p^2 = -p_\mu p^\mu$, and $x^2 = -n_\mu p^\mu$. The master function $-\Lambda(n^2, p^2, x^2)$ corresponds to the total thermodynamic energy density when neutron and proton currents flow in parallel. The stress-energy tensor in terms of the master function is written as [18,19]

$$T^\mu_\nu = \Psi\delta^\mu_\nu + n^\mu\mu_\nu + p^\mu\chi_\nu, \tag{1}$$

where

$$\Psi = \Lambda - n^{\rho}\mu_{\rho} - p^{\rho}\chi_{\rho} \tag{2}$$

is the generalized pressure, and

$$\mu_{\nu} = \mathcal{B}n_{\nu} + \mathcal{A}p_{\nu}, \tag{3}$$

$$\chi_{\nu} = \mathcal{A}n_{\nu} + \mathcal{C}p_{\nu} \tag{4}$$

are neutron and proton momentum covectors and are conjugate to n^{μ} and p^{μ}, respectively. It implies that neutron or proton momentum is a linear combination of both number density currents. The entrainment effect disappears when the coefficient $\mathcal{A}$ is zero. The magnitudes of momentum covectors μ_{ν} and χ_{ν} are chemical potentials of neutron and proton fluids, respectively [18]. The proton fluid is a charge neutral fluid made of protons and electrons [27]. For β-equilibrated neutron star matter, chemical potentials of neutron and proton fluids are the same. Consequently, the chemical potential of proton fluid is the sum of chemical potentials of protons and electrons [27,28]. Coefficients in Eqs. (3) and (4) are determined from the master function,

$$\mathcal{A} = -\frac{\partial\Lambda}{\partial x^2}\ , \qquad \mathcal{B} = -2\frac{\partial\Lambda}{\partial n^2}\ , \qquad \mathcal{C} = -2\frac{\partial\Lambda}{\partial p^2}. \tag{5}$$

The field equations for neutrons and protons involve two conservation and two Euler equations.

The master function is determined from averaged stress-energy components in a covariant way from the following relation [18,19]:

$$\Lambda = -\frac{1}{2}\langle T\rangle + \frac{3}{2}(x^4 - n^2p^2)^{-1} \times \left(n^2p^2\left[\frac{1}{n^2}n^{\mu}n^{\nu} + \frac{1}{p^2}p^{\mu}p^{\nu}\right] - x^2[n^{\mu}p^{\nu} + p^{\mu}n^{\nu}]\right)\langle T_{\mu\nu}\rangle, \tag{6}$$

where $\langle T\rangle = \langle T^{\mu}_{\mu}\rangle$ and the generalized pressure is

$$\Psi = \frac{1}{3}(\langle T\rangle - \Lambda)\ . \tag{7}$$

Similarly, one obtains the coefficients [18]

$$\mathcal{A} = \frac{-(n_{\mu}p^{\nu}\langle T^{\mu}_{\nu}\rangle + x^2\Lambda)}{(x^4 - n^2p^2)}\ , \tag{8}$$

$$\mathcal{B} = \frac{(p_{\mu}p^{\nu}\langle T^{\mu}_{\nu}\rangle + p^2\Lambda)}{(x^4 - n^2p^2)}\ , \tag{9}$$

$$\mathcal{C} = \frac{(n_{\mu}n^{\nu}\langle T^{\mu}_{\nu}\rangle + n^2\Lambda)}{(x^4 - n^2p^2)}. \tag{10}$$

Relating neutron (n^{μ}) and proton (p^{μ}) number density currents to mean particle fluxes of neutrons and protons along the z direction in the relativistic mean field (RMF) model [18], it follows from Eq. (6) that

$$\Lambda = \langle T^0_0\rangle + \langle T^z_z\rangle - \langle T^x_x\rangle\ , \tag{11}$$

where averaged stress-energy components are calculated in the RMF model and those are defined below.

Next, the implications of slow rotation are discussed in the following paragraph [18]. Here it is assumed that the space-time is flat in local regions of fluid elements. Since $x^2 - np$ is small with respect to np [18], this leads to the analytic expansion of the master function as

$$\Lambda(n^2, p^2, x^2) = \sum_{i=0}^{\infty}\lambda_i(n^2, p^2)(x^2 - np)^i\ . \tag{12}$$

Coefficients in the field equations are given by [18]

$$\mathcal{A} = -\sum_{i=1}^{\infty} i\ \lambda_i(n^2, p^2)(x^2 - np)^{i-1},$$
$$\mathcal{B} = -\frac{1}{n}\frac{\partial\lambda_0}{\partial n} - \frac{p}{n}\mathcal{A} - \frac{1}{n}\sum_{i=1}^{\infty}\frac{\partial\lambda_i}{\partial n}(x^2 - np)^i,$$
$$\mathcal{C} = -\frac{1}{p}\frac{\partial\lambda_0}{\partial p} - \frac{n}{p}\mathcal{A} - \frac{1}{p}\sum_{i=1}^{\infty}\frac{\partial\lambda_i}{\partial p}(x^2 - np)^i. \tag{13}$$

The master function is calculated within a RMF model [18,29]. In this case, the relative motion between neutrons and protons is taken into account. In the RMF model, nucleon-nucleon interaction is mediated by the exchange of mesons. Comer and Joynt [18,19] made the connection between a macroscopic fluid system and microscopic RMF model for the first time. They used the relativistic σ-ω model in their calculation [18]. However, neutron star matter is highly isospin asymmetric matter. This can be taken care of by the inclusion of ρ mesons in the RMF model. We extend the calculation of Comer and Joynt [18] to include ρ mesons as well as scalar meson self-interactions. The Lagrangian density for nucleon-nucleon interaction is given by [29]

$$\mathcal{L}_B = \sum_{B=n,p}\bar{\Psi}_B(i\gamma_{\mu}\partial^{\mu} - m_B + g_{\sigma B}\sigma - g_{\omega B}\gamma_{\mu}\omega^{\mu} - g_{\rho B}\gamma_{\mu}\boldsymbol{t}_B\cdot\rho^{\mu})\Psi_B + \frac{1}{2}(\partial_{\mu}\sigma\partial^{\mu}\sigma - m_{\sigma}^2\sigma^2) - U(\sigma) - \frac{1}{4}\omega_{\mu\nu}\omega^{\mu\nu} + \frac{1}{2}m_{\omega}^2\omega_{\mu}\omega^{\mu} - \frac{1}{4}\rho_{\mu\nu}\cdot\rho^{\mu\nu} + \frac{1}{2}m_{\rho}^2\rho_{\mu}\cdot\rho^{\mu}. \tag{14}$$

Here ψ_B denotes the Dirac bispinor for baryons B with vacuum mass m_B and the isospin operator is t_B. The scalar self-interaction term [30] is $U(\sigma) = \frac{1}{3}bm(g_\sigma\sigma)^3 + \frac{1}{4}c(g_\sigma\sigma)^4$. The Dirac nucleon effective mass m_* is defined as $m_* = m - \langle g_\sigma\sigma\rangle$. Here we use the nucleon mass (m) which is the average of bare neutron (m_n) and proton (m_p) masses. Further we use $c_\sigma^2 = (g_\sigma/m_\sigma)^2$, $c_\omega^2 = (g_\omega/m_\omega)^2$, and $c_\rho^2 = (g_\rho/m_\rho)^2$ in this calculation.

Here we adopt the mean field approximation to solve the equations of motion for meson fields [29]. We choose a frame in which neutrons have zero spatial momentum and protons have a wave vector $k_\mu = (k_0, 0, 0, K)$ [18]. We obtain the meson field equations as

$$m_* = m - c_\sigma^2\langle\bar\psi\psi\rangle + bmc_\sigma^2(m-m_*)^2 + cc_\sigma^2(m-m_*)^3 \tag{15}$$

$$g_\omega\omega_0 = -c_\omega^2(n^0 + p^0)\ , \tag{16}$$

$$g_\omega\omega^z = -c_\omega^2(n^z + p^z)\ , \tag{17}$$

$$g_\rho\rho_3^0 = -\frac{1}{2}c_\rho{}^2(p^0 - n^0)\ , \tag{18}$$

$$g_\rho\rho_3^z = -\frac{1}{2}c_\rho{}^2(p^z - n^z)\ , \tag{19}$$

where $p^0 = \langle\bar\psi_p\gamma^0\psi_p\rangle = k_p^3/3\pi^2$, $n^0 = \langle\bar\psi_n\gamma^0\psi_n\rangle = k_n^3/3\pi^2$, $p^z = \langle\bar\psi_p\gamma^z\psi_p\rangle$, and $n^z = \langle\bar\psi_n\gamma^z\psi_n\rangle$.

In the zero momentum frame of neutrons, averaged stress-energy tensor components are given by

$$\begin{aligned}\langle T_0^0\rangle = &-\frac{1}{2}c_\omega^2\sum_{B=n,p}(\langle\bar\psi_B\gamma^0\psi_B\rangle^2 - \langle\bar\psi_B\gamma^z\psi_B\rangle^2) - \frac{1}{2}c_\rho^2\sum_{B=n,p}(\langle\bar\psi_B I_{3B}\gamma^0\psi_B\rangle^2 - \langle\bar\psi_B I_{3B}\gamma^z\psi_B\rangle^2)\\ &-\frac{1}{2}c_\sigma^{-2}(m^2 - m_*^2) - \frac{1}{3}bm(m-m_*)^3 - \frac{1}{4}c(m-m_*)^4 - \sum_{B=n,p}\langle\bar\psi_B\gamma^i k_i\psi_B\rangle,\end{aligned} \tag{20}$$

$$\langle T_z^0\rangle = \sum_{B=n,p}\langle\bar\psi_B\gamma^0 k_z\psi_B\rangle, \tag{21}$$

$$\begin{aligned}\langle T_x^x\rangle &= \langle T_y^y\rangle\\ &= \frac{1}{2}c_\omega^2\sum_{B=n,p}(\langle\bar\psi_B\gamma^0\psi_B\rangle^2 - \langle\bar\psi_B\gamma^z\psi_B\rangle^2) + \frac{1}{2}c_\rho^2\sum_{B=n,p}(\langle\bar\psi_B I_{3B}\gamma^0\psi_B\rangle^2 - \langle\bar\psi_B I_{3B}\gamma^z\psi_B\rangle^2) - \frac{1}{2}c_\sigma^{-2}(m-m_*)^2\\ &\quad -\frac{1}{3}bm(m-m_*)^3 - \frac{1}{4}c(m-m_*)^4 + \sum_{B=n,p}\langle\bar\psi_B\gamma^x k_x\psi_B\rangle,\end{aligned} \tag{22}$$

$$\begin{aligned}\langle T_z^z\rangle = &\frac{1}{2}c_\omega^2\sum_{B=n,p}(\langle\bar\psi_B\gamma^0\psi_B\rangle^2 - \langle\bar\psi_B\gamma^z\psi_B\rangle^2) + \frac{1}{2}c_\rho^2\sum_{B=n,p}(\langle\bar\psi_B I_{3B}\gamma^0\psi_B\rangle^2 - \langle\bar\psi_B I_{3B}\gamma^z\psi_B\rangle^2) - \frac{1}{2}c_\sigma^{-2}(m-m_*)^2\\ &-\frac{1}{3}bm(m-m_*)^3 - \frac{1}{4}c(m-m_*)^4 + \sum_{B=n,p}\langle\bar\psi_B\gamma^z k_z\psi_B\rangle,\end{aligned} \tag{23}$$

where I_{3B} is the third isospin component for baryon B. Averaged stress-energy tensor components include terms which are to be integrated over neutron and proton Fermi surfaces.

We perform integrations in cylindrical coordinates with the definitions $\phi_\omega = g_\omega\omega^z$, $\phi_{\omega K} = \phi_\omega + K$, and $\phi_\rho = g_\rho\rho_3^z$ as in Ref. [18]. We write the effective mass explicitly as

$$\begin{aligned}m_* = m - \frac{c_\sigma^2}{2\pi^2}m_*\Bigg(&\int_{-k_n}^{k_n}dk_z\left[k_n^2 + \phi_\omega^2 + \frac{1}{4}\phi_\rho^2 + m_*^2 + 2\phi_\omega k_z - \phi_\rho k_z - \phi_\omega\phi_\rho\right]^{1/2}\\ &+\int_{-k_p}^{k_p}dk_z\left[k_p^2 + \left(\phi_{\omega K} + \frac{1}{2}\phi_\rho\right)^2 + m_*^2 + 2\left(\phi_{\omega K} + \frac{1}{2}\phi_\rho\right)k_z\right]^{1/2}\\ &-\int_{-k_n}^{k_n}dk_z\left[\left(k_z + \phi_\omega - \frac{1}{2}\phi_\rho\right)^2 + m_*^2\right]^{1/2} - \int_{-k_p}^{k_p}dk_z\left[\left(k_z + \phi_{\omega K} + \frac{1}{2}\phi_\rho\right)^2 + m_*^2\right]^{1/2}\Bigg)\\ &+bmc_\sigma^2(m-m_*)^2 + cc_\sigma^2(m-m_*)^3.\end{aligned} \tag{24}$$

The z components of neutron and proton number current densities take the form

$$n^z = \frac{1}{2\pi^2}\int_{-k_n}^{k_n} dk_z \left(k_z + \phi_\omega - \frac{1}{2}\phi_\rho\right)\left(\left[k_n^2 + m_*^2 + \phi_\omega^2 - \frac{1}{4}\phi_\rho^2 + 2\phi_\omega k_z - \phi_\rho k_z\right]^{1/2} - \left[\left(k_z + \phi_\omega - \frac{1}{2}\phi_\rho\right)^2 + m_*^2\right]^{1/2}\right),$$
$$p^z = \frac{1}{2\pi^2}\int_{-k_p}^{k_p} dk_z \left(k_z + \phi_{\omega K} + \frac{1}{2}\phi_\rho\right)\left(\left[k_p^2 + m_*^2 + \left(\phi_{\omega K} + \frac{1}{2}\phi_\rho\right)^2 + 2\left(\phi_{\omega K} + \frac{1}{2}\phi_\rho\right)k_z\right]^{1/2} - \left[\left(k_z + \phi_{\omega K} + \frac{1}{2}\phi_\rho\right)^2 + m_*^2\right]^{1/2}\right). \quad (25)$$

The master function in Eq. (6) can be written as [19]

$$\Lambda = -\frac{c_\omega^2}{18\pi^4}(k_n^3 + k_p^3)^2 - \frac{c_\rho^2}{72\pi^4}(k_p^3 - k_n^3)^2 - \frac{1}{2c_\omega^2}\phi_\omega^2 - \frac{1}{2c_\rho^2}\phi_\rho^2 - \frac{1}{2c_\sigma^2}(m^2 - m_*^2) - \frac{1}{3}bm(m - m_*)^3 - \frac{1}{4}c(m - m_*)^4 - 3\sum_{B=n,p}\langle\bar{\psi}_B\gamma^x k_x\psi_B\rangle\ , \quad (26)$$

where

$$\sum_{B=n,p}\langle\bar{\psi}_B\gamma^x k_x\psi_B\rangle = \frac{1}{12\pi^2}\left(\int_{-k_n}^{k_n} dk_z\left[\left(k_n^2 - 2m_*^2 - 2\phi_\omega^2 - \frac{1}{2}\phi_\rho^2 - 3k_z^2 - 4\phi_\omega k_z + 2\phi_\rho k_z + 2\phi_\omega\phi_\rho\right)\right.\right.$$
$$\times\left(k_n^2 + \phi_\omega^2 + \frac{1}{4}\phi_\rho^2 + m_*^2 + 2\phi_\omega k_z - \phi_\rho k_z - \phi_\omega\phi_\rho\right)^{1/2} + 2\left(\left[k_z + \phi_\omega - \frac{1}{2}\phi_\rho\right]^2 + m_*^2\right)^{3/2}\Big]$$
$$+\int_{-k_p}^{k_p} dk_z\left[\left(k_p^2 - 2m_*^2 - 2\phi_{\omega K}^2 - \frac{1}{2}\phi_\rho^2 - 3k_z^2 - 4\phi_{\omega K}k_z - 2\phi_\rho k_z - 2\phi_{\omega K}\phi_\rho\right)\right.$$
$$\left.\left.\times\left(k_p^2 + \phi_{\omega K}^2 + \frac{1}{4}\phi_\rho^2 + m_*^2 + 2\phi_{\omega K}k_z + \phi_\rho k_z + \phi_{\omega K}\phi_\rho\right)^{1/2} + 2\left(\left[k_z + \phi_{\omega K} + \frac{1}{2}\phi_\rho\right]^2 + m_*^2\right)^{3/2}\right]\right). \quad (27)$$

In evaluating the master function, as well as the coefficients, the slow rotation approximation which implies that K should be small compared with $k_{n,p}$ is exploited, as detailed in the Appendix. We are dealing with superfluidity in neutron star matter which is made of neutrons, protons, and electrons. When we neglect the relative motion between neutron and proton fluids, $-\Lambda|_0$ becomes the energy density of the neutron star matter. We add the contribution of electrons to the master function (Λ). Here, electrons are treated as noninteracting relativistic particles. Therefore, in the limit $K \to 0$, the master function which is the first term of Eq. (12), generalized pressure, and the chemical potentials of neutron and proton fluids are given by

$$\Lambda|_0 = -\frac{c_\omega^2}{18\pi^4}(k_n^3 + k_p^3)^2 - \frac{c_\rho^2}{72\pi^4}(k_p^3 - k_n^3)^2 - \frac{1}{4\pi^2}\left(k_n^3\sqrt{k_n^2 + m_*^2|_0} + k_p^3\sqrt{k_p^2 + m_*^2|_0}\right)$$
$$-\frac{1}{4}c_\sigma^{-2}[(2m - m_*|_0)(m - m_*|_0) + m_*|_0(bmc_\sigma^2(m - m_*|_0)^2 + cc_\sigma^2(m - m_*|_0)^3)]$$
$$-\frac{1}{8\pi^2}\left(k_p[2k_p^2 + m_e^2]\sqrt{k_p^2 + m_e^2} - m_e^4 ln\left[\frac{k_p + \sqrt{k_p^2 + m_e^2}}{m_e}\right]\right), \quad (28)$$

$$\mu|_0 = -\frac{\pi^2}{k_n^2}\frac{\partial\Lambda}{\partial k_n}\bigg|_0 = \frac{c_\omega^2}{3\pi^2}(k_n^3 + k_p^3) - \frac{c_\rho^2}{12\pi^2}(k_p^3 - k_n^3) + \sqrt{k_n^2 + m_*^2|_0}, \quad (29)$$

$$\chi|_0 = -\frac{\pi^2}{k_p^2}\frac{\partial\Lambda}{\partial k_p}\bigg|_0 = \frac{c_\omega^2}{3\pi^2}(k_n^3+k_p^3) + \frac{c_\rho^2}{12\pi^2}(k_p^3-k_n^3) + \sqrt{k_p^2+m_*^2|_0} + \sqrt{k_p^2+m_e^2}, \tag{30}$$

$$\Psi|_0 = \Lambda|_0 + \frac{1}{3\pi^2}(\mu|_0 k_n^3 + \chi|_0 k_p^3)\ , \tag{31}$$

where the subscript "0" stands for quantities calculated in the limit $K \to 0$. It is to be noted here that energy density $-\Lambda|_0$ and pressure $\Psi|_0$ constitute the equation of state for the calculation of equilibrium configurations of neutron stars which we discuss in Sec. III.

Coefficients in momentum covectors are given by

$$\begin{aligned}\mathcal{A}|_0 = {} & c_\omega^2 - \frac{1}{4}c_\rho^2 + \frac{c_\omega^2}{5\mu^2|_0}\left(2k_p^2\frac{\sqrt{k_n^2+m_*^2|_0}}{\sqrt{k_p^2+m_*^2|_0}} + \frac{c_\omega^2}{3\pi^2}\left[\frac{k_n^2k_p^3}{\sqrt{k_n^2+m_*^2|_0}} + \frac{k_p^2k_n^3}{\sqrt{k_p^2+m_*^2|_0}}\right]\right) \\ & + \frac{c_\rho^2}{20\mu^2|_0}\left(2k_p^2\frac{\sqrt{k_n^2+m_*^2|_0}}{\sqrt{k_p^2+m_*^2|_0}} + \frac{c_\rho^2}{12\pi^2}\left[\frac{k_n^2k_p^3}{\sqrt{k_n^2+m_*^2|_0}} + \frac{k_p^2k_n^3}{\sqrt{k_p^2+m_*^2|_0}}\right]\right) - \frac{c_\rho^2c_\omega^2}{30\mu^2|_0\pi^2}\left[\frac{k_n^2k_p^3}{\sqrt{k_n^2+m_*^2|_0}} - \frac{k_p^2k_n^3}{\sqrt{k_p^2+m_*^2|_0}}\right] \\ & + \frac{3\pi^2k_p^2}{5\mu^2|_0k_n^3}\frac{k_n^2+m_*^2|_0}{\sqrt{k_p^2+m_*^2|_0}},\end{aligned} \tag{32}$$

$$\begin{aligned}\mathcal{B}|_0 = {} & \frac{3\pi^2\mu|_0}{k_n^3} - c_\omega^2\frac{k_p^3}{k_n^3} + \frac{1}{4}c_\rho^2\frac{k_p^3}{k_n^3} - \frac{c_\omega^2k_p^3}{5\mu^2|_0k_n^3}\left(2k_p^2\frac{\sqrt{k_n^2+m_*^2|_0}}{\sqrt{k_p^2+m_*^2|_0}} + \frac{c_\omega^2}{3\pi^2}\left[\frac{k_n^2k_p^3}{\sqrt{k_n^2+m_*^2|_0}} + \frac{k_p^2k_n^3}{\sqrt{k_p^2+m_*^2|_0}}\right]\right) \\ & - \frac{c_\rho^2k_p^3}{20\mu^2|_0k_n^3}\left(2k_p^2\frac{\sqrt{k_n^2+m_*^2|_0}}{\sqrt{k_p^2+m_*^2|_0}} + \frac{c_\rho^2}{12\pi^2}\left[\frac{k_n^2k_p^3}{\sqrt{k_n^2+m_*^2|_0}} + \frac{k_p^2k_n^3}{\sqrt{k_p^2+m_*^2|_0}}\right]\right) \\ & + \frac{c_\rho^2c_\omega^2k_p^3}{30\pi^2\mu^2|_0k_n^3}\left[\frac{k_n^2k_p^3}{\sqrt{k_n^2+m_*^2|_0}} - \frac{k_p^2k_n^3}{\sqrt{k_p^2+m_*^2|_0}}\right] - \frac{3\pi^2k_p^5}{5\mu^2|_0k_n^6}\frac{k_n^2+m_*^2|_0}{\sqrt{k_p^2+m_*^2|_0}},\end{aligned} \tag{33}$$

$$\begin{aligned}\mathcal{C}|_0 = {} & \frac{3\pi^2\chi|_0}{k_p^3} + \frac{1}{4}c_\rho^2\frac{k_n^3}{k_p^3} - c_\omega^2\frac{k_n^3}{k_p^3} - \frac{c_\omega^2k_n^3}{5\mu^2|_0k_p^3}\left(2k_p^2\frac{\sqrt{k_n^2+m_*^2|_0}}{\sqrt{k_p^2+m_*^2|_0}} + \frac{c_\omega^2}{3\pi^2}\left[\frac{k_n^2k_p^3}{\sqrt{k_n^2+m_*^2|_0}} + \frac{k_p^2k_n^3}{\sqrt{k_p^2+m_*^2|_0}}\right]\right) \\ & - \frac{c_\rho^2k_n^3}{20\mu^2|_0k_p^3}\left(2k_p^2\frac{\sqrt{k_n^2+m_*^2|_0}}{\sqrt{k_p^2+m_*^2|_0}} + \frac{c_\rho^2}{12\pi^2}\left[\frac{k_n^2k_p^3}{\sqrt{k_n^2+m_*^2|_0}} + \frac{k_p^2k_n^3}{\sqrt{k_p^2+m_*^2|_0}}\right]\right) \\ & + \frac{c_\rho^2c_\omega^2k_n^3}{30\pi^2\mu^2|_0k_p^3}\left[\frac{k_n^2k_p^3}{\sqrt{k_n^2+m_*^2|_0}} - \frac{k_p^2k_n^3}{\sqrt{k_p^2+m_*^2|_0}}\right] - \frac{3\pi^2}{5\mu^2|_0k_p}\frac{k_n^2+m_*^2|_0}{\sqrt{k_p^2+m_*^2|_0}}\ .\end{aligned} \tag{34}$$

Similarly, other coefficients which enter into the calculation of equilibrium neutron star configurations are calculated according to Ref. [18] and given by

$$\mathcal{A}_0^0|_0 = -\frac{\pi^4}{k_p^2k_n^2}\frac{\partial^2\Lambda}{\partial k_p\partial k_n}\bigg|_0 = c_\omega^2 - \frac{c_\rho^2}{4} + \frac{\pi^2}{k_p^2}\frac{m_*|_0\frac{\partial m_*}{\partial k_p}|_0}{\sqrt{k_n^2+m_*^2|_0}}, \tag{35}$$

$$\mathcal{B}_0^0|_0 = \frac{\pi^4}{k_n^5}\left(2\frac{\partial\Lambda}{\partial k_n}\bigg|_0 - k_n\frac{\partial^2\Lambda}{\partial k_n^2}\bigg|_0\right) = c_\omega^2 + \frac{c_\rho^2}{4} + \frac{\pi^2}{k_n^2}\frac{k_n + m_*|_0\frac{\partial m_*}{\partial k_n}|_0}{\sqrt{k_n^2+m_*^2|_0}}, \tag{36}$$

$$\mathcal{C}_0^0|_0 = \frac{\pi^4}{k_p^5}\left(2\frac{\partial\Lambda}{\partial k_p}\Big|_0 - k_p\frac{\partial^2\Lambda}{\partial k_p^2}\Big|_0\right)$$
$$= c_\omega^2 + \frac{c_\rho^2}{4} + \frac{\pi^2}{k_p^2}\frac{k_p + m_*|_0\frac{\partial m_*}{\partial k_p}|_0}{\sqrt{k_p^2+m_*^2|_0}} + \frac{\pi^2}{k_p}\frac{1}{\sqrt{k_p^2+m_e^2}}\ . \quad (37)$$

Derivatives of the effective mass with respect to neutron and proton Fermi momenta are explicitly shown in the Appendix.

We obtain entrainment matrix elements inverting Eqs. (3) and (4) and compare those with the relativistic analog of the mass density matrix (ρ_{ik}) [18,31]:

$$Y_{nn} = \frac{\rho_{nn}}{m^2} = \frac{\mathcal{C}|_0}{(\mathcal{B}|_0\mathcal{C}|_0 - \mathcal{A}|_0^2)},$$
$$Y_{np} = \frac{\rho_{np}}{m^2} = -\frac{\mathcal{A}|_0}{(\mathcal{B}|_0\mathcal{C}|_0 - \mathcal{A}|_0^2)},$$
$$Y_{pp} = \frac{\rho_{pp}}{m^2} = \frac{\mathcal{B}|_0}{(\mathcal{B}|_0\mathcal{C}|_0 - \mathcal{A}|_0^2)}. \quad (38)$$

The entrainment matrix in this form can be compared with that of Ref. [17]. It is worth noting here that when Eqs. (3) and (4) are inverted and neutron and proton number density currents are written in terms of chemical potentials, we obtain the relation $\sum_{k=n,p} Y_{ik}\mu_k = n_i$, where $i = n,\ p$.

Now the entrainment parameter ($\varepsilon_{\rm mom}$) in the zero momentum frame of neutrons is related to the off-diagonal component of the mass density matrix, i.e., $\rho_{np} = -\varepsilon_{\rm mom} mn$, and can be calculated in terms of coefficients in momentum covectors in two-fluid formalism from the following relation [18]:

$$\varepsilon_{\rm mom} = \frac{m}{n}\frac{\mathcal{A}|_0}{(\mathcal{B}|_0\mathcal{C}|_0 - \mathcal{A}|_0^2)}\ . \quad (39)$$

Similarly, the entrainment parameter in the zero velocity frame of neutrons is given by [7,18]

$$\varepsilon_{\rm vel} = \frac{\mathcal{A}|_0 n}{m}\ . \quad (40)$$

In the nonrelativistic case, an explicit relationship between the entrainment parameter and effective nucleon mass was found by various groups [7,15].

Finally, charge neutrality and β-equilibrium conditions are to be imposed in neutron star matter. The charge neutrality condition is $k_p = k_e$. The condition of chemical equilibrium for npe matter is $\mu|_0 = \chi|_0$, where $\mu|_0$ and $\chi|_0$ are the neutron and proton plus electron chemical potentials, respectively.

TABLE I. Nucleon-meson coupling constants in the GL and NL3 sets are taken from Refs. [29,33]. The coupling constants are obtained by reproducing the saturation properties of symmetric nuclear matter as detailed in the text. All the parameters are in fm^2, except b and c which are dimensionless.

	c_σ^2	c_ω^2	c_ρ^2	b	c
GL	12.684	7.148	4.410	0.005610	−0.006986
NL3	15.739	10.530	5.324	0.002055	−0.002650

III. RESULTS AND DISCUSSION

Meson-nucleon couplings c_σ, c_ω, c_ρ, b, and c of the Lagrangian density in Eq. (14) are determined by reproducing nuclear matter saturation properties such as binding energy per nucleon (−16.3 MeV), saturation density ($n_0 = 0.153$ fm^{-3}), Dirac nucleon effective mass ($m_*/m = 0.7$), the symmetry energy coefficient (32.5 MeV), and incompressibility (200 MeV). These coupling constants are taken from Ref. [29]. This parameter set is known as the Glendenning (GL) set. We also perform the calculation using the non-linear (NL3) interaction [32]. New parametrization of the NL3 interaction, reproducing binding energy per nucleon (−16.24 MeV), saturation density (0.148 fm^{-3}), incompressibility (271.5 MeV), the symmetry energy coefficient (37.29 MeV), and the slope of the symmetry energy (118.2 MeV) [33], is adopted in our calculation. Both parameter sets are listed in Table I.

In this calculation, we consider the β-equilibrated neutron star matter made of neutrons (n), protons (p), and electrons (e). Equilibrium configurations of neutron stars are calculated following the prescription of Comer and other collaborators [18,27] and using our equation of state as given by energy density ($-\Lambda|_0$) and pressure ($\Psi|_0$) in Eqs. (28) and (31), respectively. Neutron and proton Fermi momenta at the center of the star are needed for this purpose. For a given value of neutron Fermi momentum or wave number, proton Fermi momentum is calculated from the β-equilibrium condition. We perform this calculation for the GL and NL3 parameter sets. Neutron star masses as a function of central neutron density for NL3 (solid line) and GL (dashed line) sets are plotted in Fig. 1. It is noted that maximum neutron star masses corresponding to the GL and NL3 parameters are well above the observed limit of 2.01 ± 0.04 M$_\odot$ [34]. For the calculation of entrainment, we choose neutron star configurations which are just below maximum masses in both cases. In the case of the GL set, we consider a neutron star mass of 2.37 M$_\odot$ corresponding to the central value of neutron wave number $k_n(0) = 2.71$ fm^{-1} and proton fraction 0.24. The radius of the neutron star is 11.09 km. Similarly, in the other case with the NL3 set, we find a neutron star having maximum mass 2.82 M$_\odot$ and radius 13.17 km. The corresponding central values of the neutron wave number and proton fraction are 2.40 fm^{-1} and 0.23, respectively.

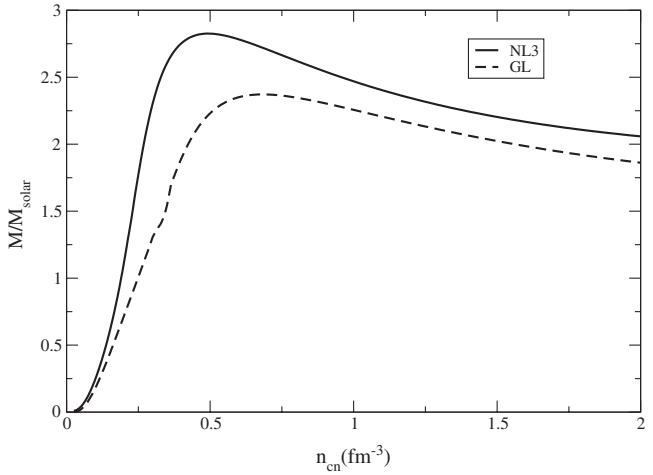

FIG. 1. Neutron star sequence is plotted with central neutron density. The dashed line corresponds to the calculation with the GL parameter set, whereas the solid line implies that of the NL3 parameter set.

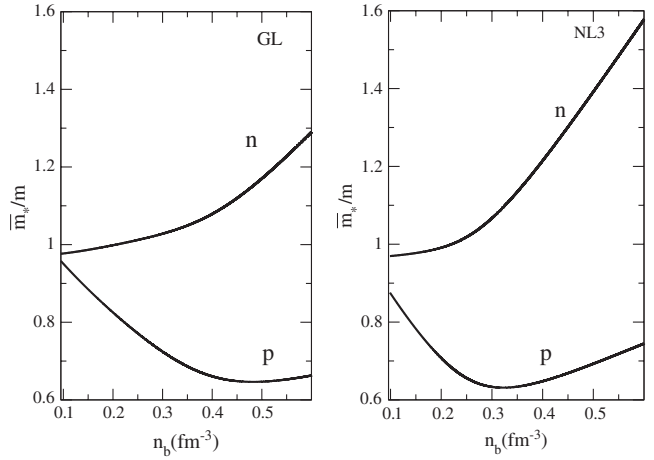

FIG. 2. Dynamical neutron and proton effective masses are shown as a function of baryon density for the GL (left panel) and NL3 (right panel) parameter sets.

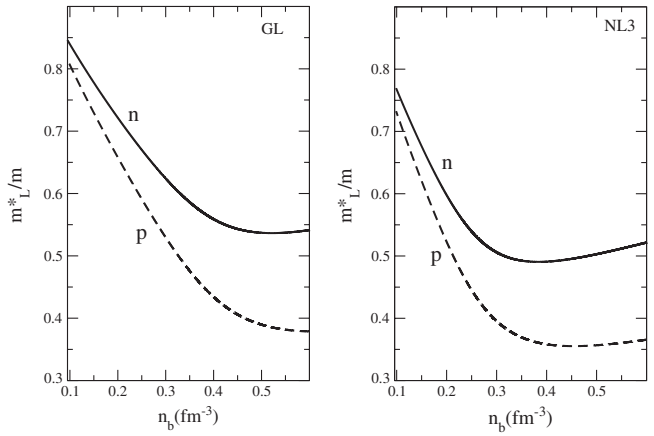

FIG. 3. Landau effective masses are shown as a function of baryon density for the GL (left panel) and NL3 (right panel) parameter sets.

We calculate dynamical neutron and proton effective masses [9] using $\bar{m}_*^n = n_n \mathcal{B}|_0$ and $\bar{m}_*^p = n_p \mathcal{C}|_0$, where n_n and n_p are neutron and proton number densities. Dynamical effective masses are plotted as a function of baryon density in Fig. 2. The left panel shows the results of the GL parameter set, whereas the right panel denotes those of the NL3 parameter set. In both panels, the upper curve represents the neutron effective mass and the lower curve corresponds to the proton effective mass. It is noted that the neutron effective mass increases with density and becomes greater than the free neutron mass in both cases. However, it rises faster in the NL3 case. On the other hand, the proton effective mass decreases with density initially and rises at higher densities. However, its value always stays below the free proton mass. In the GL case, the proton effective mass is always higher than that of the NL3 case. These findings are different from the effective masses calculated in the nonrelativistic calculations, as noted already in Refs. [9,15].

We also calculate the Landau effective mass for nucleons and it is related to the Dirac effective mass through the expression $m_L^{*i} = \sqrt{k_i^2 + (m - g_\sigma \sigma)^2}$ [17]. Landau effective masses for neutrons and protons are shown as a function of baryon density in Fig. 3. The left panel shows the results of the GL set and the right panel represents those of the NL3 set. Here we find that neutron and proton effective masses decrease as baryon density increases in both panels, and they are below their bare masses. It is noted that the Landau effective masses are always higher in the GL set than those of the NL3 set.

Normalized entrainment matrix elements of Eq. (38) are shown as a function of baryon density in Fig. 4. The normalization constant is chosen as $Y = 3n_0/\mu_n(3n_0)$, as done in Ref. [17]. Entrainment matrix elements obtained in this calculation are compared with those calculated in the relativistic Landau Fermi liquid theory [17]. Both calculations are performed using the GL set of Table I. Solid lines represent the results of Ref. [17], whereas dashed lines demonstrate the results of Eq. (38) using the GL set. Though the results of the two calculations are qualitatively similar, they are quantitatively very different. The difference between the results of the two calculations is negligible initially, because the entrainment effect becomes small in the low density region in both approaches. On the other hand, this difference grows at higher baryon densities as the entrainment effect becomes more dominant in our case than that of Ref. [17]. This may be attributed to different formalisms in two calculations. We also compare normalized matrix elements calculated in our model using the GL and NL3 parameter sets in Fig. 5. Results of the

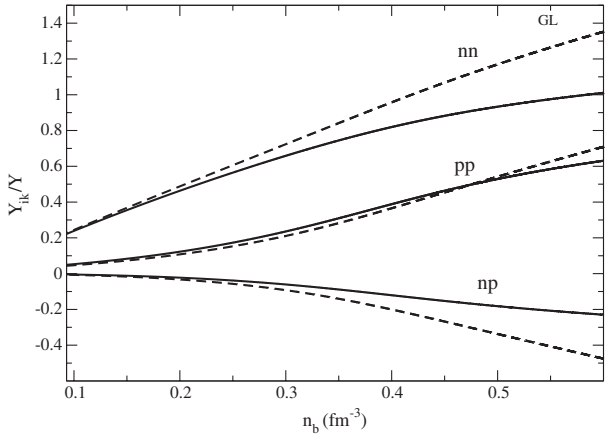

FIG. 4. Normalized entrainment matrix elements (Y_{ik}/Y) in the zero momentum frame are plotted as a function of baryon density. The normalization factor is taken as $Y = 3n_0/\mu_n(3n_0)$ [17], where n_0 is the saturation density. Results of this calculation (dashed line) are compared with those (solid line) of Ref. [17].

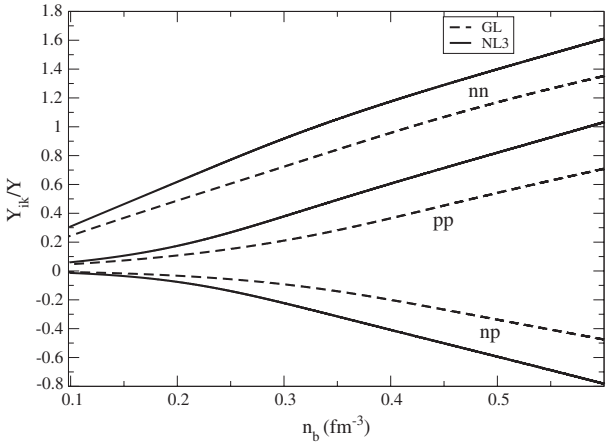

FIG. 5. Normalized entrainment matrix elements (Y_{ik}/Y) in the zero momentum frame are plotted as a function of baryon density for the GL and NL3 parameter sets. The normalization factor is taken as $Y = 3n_0/\mu_n(3n_0)$ [17], where n_0 is the saturation density.

NL3 set are higher than those of the GL set. The difference in the equations of state for the two parameter sets is reflected in the results of matrix element calculations.

Next we present the results of entrainment parameters in the zero momentum and zero velocity frames of neutrons. The radial profiles of the entrainment parameter in the zero momentum frame for the GL and NL3 sets are shown in Fig. 6. These radial profiles are obtained for neutron stars of mass $M = 2.37\ \mathrm{M}_\odot$ and radius $R = 11.09$ km in the case of the GL set and $M = 2.82\,\mathrm{M}_\odot$ and radius $R = 13.17$ km in the case of the NL3 set. The entrainment parameter in both cases remains constant in the core and drops rapidly at the surface. We find an appreciable difference between the two results towards the center. Moreover, in both cases, the entrainment effect is strong at higher baryon densities in

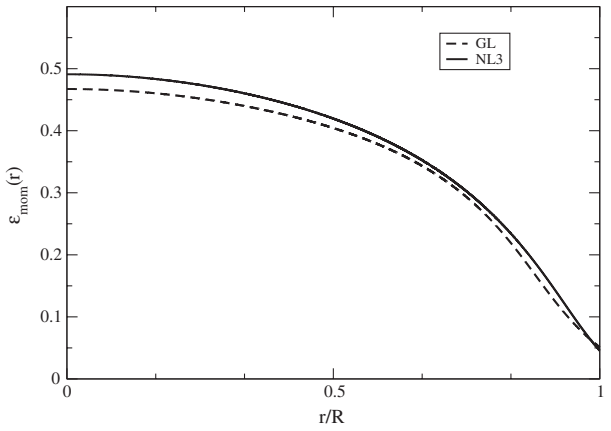

FIG. 6. Entrainment parameter in the RMF model with ρ mesons in the zero momentum frame of neutrons is plotted as a function of radial distance in a neutron star of mass 2.37 $\mathrm{M}_\odot$ and radius 11.09 km using the GL parameter set (dashed line) and mass 2.82 $\mathrm{M}_\odot$ and radius 13.17 km with the NL3 parameter set (solid line).

the core, whereas this effect diminishes sharply at lower densities towards the surface. The value of the entrainment parameter lies in the physical range $0 \le \varepsilon_{\mathrm{mom}} \le 1$ as found in earlier calculations [7,15]. We compare this result with that of the situation excluding ρ mesons, which was actually studied in Ref. [18], as displayed in Fig. 7 for the GL set. For the calculation of the entrainment parameter without ρ mesons, we obtain the radial profile of the entrainment parameter in a neutron star of mass 2.33 $\mathrm{M}_\odot$ and radius 10.96 km. It is evident from Figs. 6 and 7 that the inclusion of ρ in the calculation strongly enhances the entrainment parameter.

Further, the radial profile of the entrainment parameter ($\varepsilon_{\mathrm{vel}}$) in the zero velocity frame is exhibited in Fig. 8. The solid line denotes the calculation without ρ mesons and the dashed line implies the case including ρ mesons. It is noted

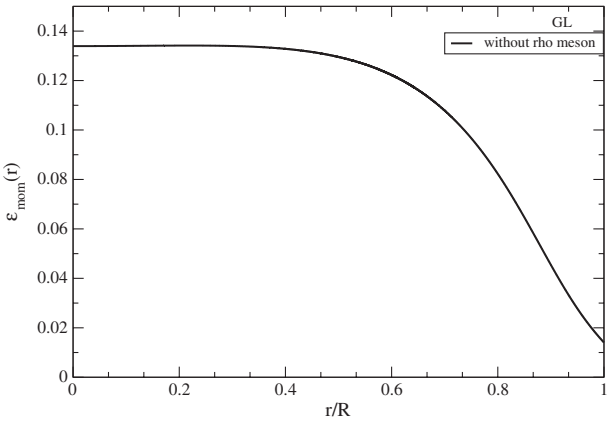

FIG. 7. Entrainment parameter in the RMF model without ρ mesons in the zero momentum frame of neutrons is plotted as a function of radial distance in a neutron star of mass 2.33 $\mathrm{M}_\odot$ and radius 10.96 km.

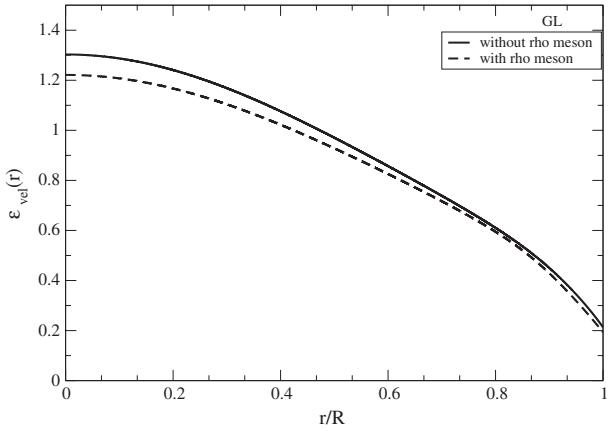

FIG. 8. Entrainment parameter in the zero velocity frame of neutrons is plotted as a function of radial distance in neutron stars of masses 2.33 $M_\odot$ (solid line) and 2.37 $M_\odot$ (dashed line).

that the entrainment parameter calculated without ρ mesons is larger compared with the entrainment parameter with ρ mesons. This finding is opposite to what we see in the calculation of the entrainment parameter in the zero momentum frame. We also find that the values of the entrainment parameter in the zero velocity frame are higher than those of the entrainment parameter in the zero momentum frame. Finally, we compare the radial profiles of entrainment parameters in the zero velocity frame for the GL and NL3 parameter sets, as shown in Fig. 9. It is evident from the figure that the two results do not differ much.

So far we have neglected muons in our calculation. However, muons can be populated in neutron star matter when the threshold condition involving electron and muon chemical potentials, $\mu_e = \mu_\mu$, is satisfied. We repeat our calculation including muons. However, muons have negligible effects on the entrainment matrix elements and entrainment parameter.

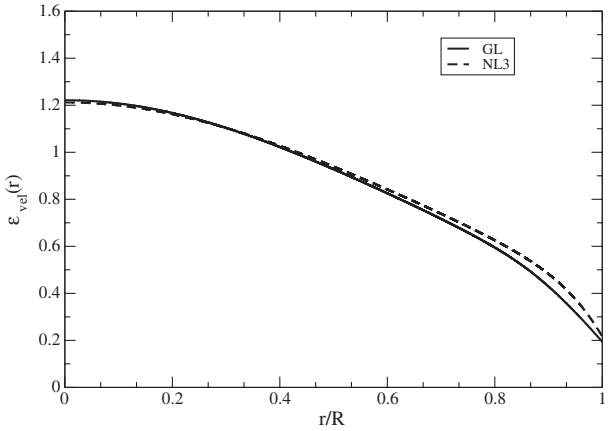

FIG. 9. Entrainment parameter in the zero velocity frame of neutrons is plotted as a function of radial distance in neutron stars of masses 2.37 $M_\odot$ (solid line) and 2.82 $M_\odot$ (dashed line) for the GL and NL3 parameter sets, respectively.

IV. SUMMARY AND CONCLUSIONS

We have extended the calculation of Comer and Joynt [18] to include ρ mesons and the self-interaction term in the RMF model. Here we calculate entrainment matrix elements and entrainment parameters using this model and the GL and NL3 parameter sets. It is noted that the entrainment parameter in the zero momentum frame is significantly enhanced due to the presence of ρ mesons in the calculation. Furthermore, we compare our results with those of the relativistic Landau Fermi liquid theory [17] and find appreciable differences.

Our calculation may be extended to include hyperons in a straightforward manner using a three-fluid description [8] and applied to study the dynamics of superfluid neutron stars. This could be compared with the findings of earlier calculations including hyperons in the relativistic Landau Fermi liquid theory [17,35].

APPENDIX

In the slow rotation approximation, we expand scalar and vector quantities in terms of K. Scalar quantities like m_* and Λ depend on even powers of K, whereas vector quantities depend on odd powers of K. We keep terms up to K^2 in our calculation. Effective mass, z components of ω and ρ fields are expanded in the following way [18]:

$$\phi_\omega = \left.\frac{\partial\phi_\omega}{\partial K}\right|_0 K,$$
$$\phi_\rho = \left.\frac{\partial\phi_\rho}{\partial K}\right|_0 K,$$
$$m_* = m_*|_0 + \left.\frac{\partial m_*}{\partial K^2}\right|_0 K^2. \tag{A1}$$

Here,

$$\begin{aligned} m_*|_0 &= m_*(k_n, k_p, 0) \\ &= m - m_*|_0 \frac{c_\sigma^2}{2\pi^2}\left(k_n\sqrt{k_n^2 + m_*^2|_0} + k_p\sqrt{k_p^2 + m_*^2|_0}\right. \\ &\quad + \frac{1}{2}m_*^2|_0 \ln\left[\frac{-k_n + \sqrt{k_n^2 + m_*^2|_0}}{k_n + \sqrt{k_n^2 + m_*^2|_0}}\right] \\ &\quad \left. + \frac{1}{2}m_*^2|_0 \ln\left[\frac{-k_p + \sqrt{k_p^2 + m_*^2|_0}}{k_p + \sqrt{k_p^2 + m_*^2|_0}}\right]\right) \\ &\quad + bmc_\sigma^2(m - m_*)^2 + cc_\sigma^2(m - m_*)^3. \end{aligned} \tag{A2}$$

Plugging Eq. (A1)) in Eqs. (24) and (25), and expanding and keeping terms up to orders K^2, we obtain

$$\left.\frac{\partial m_*}{\partial k_n}\right|_0 = -\frac{c_\sigma^2}{\pi^2}\frac{m_*|_0 k_n^2}{\sqrt{k_n^2+m_*^2|_0}}\left(\frac{3m-2m_*|_0+3bmc_\sigma^2(m-m_*|_0)^2+3cc_\sigma^2(m-m_*|_0)^3}{m_*|_0}\right.$$
$$\left.-\frac{c_\sigma^2}{\pi^2}\left[\frac{k_n^3}{\sqrt{k_n^2+m_*^2|_0}}+\frac{k_p^3}{\sqrt{k_p^2+m_*^2|_0}}\right]+2bmc_\sigma^2(m-m_*|_0)+3cc_\sigma^2(m-m_*|_0)^2\right)^{-1}, \tag{A3}$$

$$\left.\frac{\partial m_*}{\partial k_p}\right|_0 = -\frac{c_\sigma^2}{\pi^2}\frac{m_*|_0 k_p^2}{\sqrt{k_p^2+m_*^2|_0}}\left(\frac{3m-2m_*|_0+3bmc_\sigma^2(m-m_*|_0)^2+3cc_\sigma^2(m-m_*|_0)^3}{m_*|_0}\right.$$
$$\left.-\frac{c_\sigma^2}{\pi^2}\left[\frac{k_n^3}{\sqrt{k_n^2+m_*^2|_0}}+\frac{k_p^3}{\sqrt{k_p^2+m_*^2|_0}}\right]+2bmc_\sigma^2(m-m_*|_0)+3cc_\sigma^2(m-m_*|_0)^2\right)^{-1}, \tag{A4}$$

$$n^z = \frac{1}{3\pi^2}\frac{k_n^3}{\sqrt{k_n^2+m_*^2|_0}}\left(\left.\frac{\partial\phi_\omega}{\partial K}\right|_0 K-\frac{1}{2}\left.\frac{\partial\phi_\rho}{\partial K}\right|_0 K\right), \tag{A5}$$

$$p^z = \frac{1}{3\pi^2}\frac{k_p^3}{\sqrt{k_p^2+m_*^2|_0}}\left(\left.\frac{\partial\phi_\omega}{\partial K}\right|_0 K+\frac{1}{2}\left.\frac{\partial\phi_\rho}{\partial K}\right|_0 K+K\right), \tag{A6}$$

and also

$$p^z+n^z = -\frac{1}{c_\omega^2}\left.\frac{\partial\phi_\omega}{\partial K}\right|_0 K \tag{A7}$$

$$p^z-n^z = -\frac{2}{c_\rho^2}\left.\frac{\partial\phi_\rho}{\partial K}\right|_0 K. \tag{A8}$$

Using the four equations above, we get

$$\left.\frac{\partial\varphi_z}{\partial K}\right|_0 = \frac{-\frac{c_\omega^2}{3\pi^2}\frac{k_p^3}{\sqrt{k_p^2+m_*^2|_0}}\left(1+\frac{1}{4}\frac{c_\rho^2}{3\pi^2}\frac{2k_n^3}{\sqrt{k_n^2+m_*^2|_0}}\right)}{\left(1+\frac{c_\omega^2+\frac{c_\rho^2}{4}}{3\pi^2}\left[\frac{k_n^3}{\sqrt{k_n^2+m_*^2|_0}}+\frac{k_p^3}{\sqrt{k_p^2+m_*^2|_0}}\right]+\frac{c_\omega^2c_\rho^2}{9\pi^4}\left[\frac{k_n^3k_p^3}{\sqrt{(k_n^2+m_*^2|_0)(k_p^2+m_*^2|_0)}}\right]\right)}, \tag{A9}$$

$$\frac{1}{2}\left.\frac{\partial\phi_\rho}{\partial K}\right|_0 = \frac{-\frac{1}{4}\frac{c_\rho^2}{3\pi^2}\frac{k_p^3}{\sqrt{k_p^2+m_*^2|_0}}\left(1+\frac{c_\omega^2}{3\pi^2}\frac{2k_n^3}{\sqrt{k_n^2+m_*^2|_0}}\right)}{\left(1+\frac{c_\omega^2+\frac{c_\rho^2}{4}}{3\pi^2}\left[\frac{k_n^3}{\sqrt{k_n^2+m_*^2|_0}}+\frac{k_p^3}{\sqrt{k_p^2+m_*^2|_0}}\right]+\frac{c_\omega^2c_\rho^2}{9\pi^4}\left[\frac{k_n^3k_p^3}{\sqrt{(k_n^2+m_*^2|_0)(k_p^2+m_*^2|_0)}}\right]\right)} \tag{A10}$$

Further, we find $\left.\frac{\partial m_*}{\partial K^2}\right|_0 = 0$.

[1] C. O. Heinke and W. C. G. Ho, Astrophys. J. Lett. **719**, L167 (2010).

[2] D. Page, M. Prakash, J. M. Lattimer, and A. W. Steiner, Phys. Rev. Lett. **106**, 081101 (2011); P. S. Shternin, D. G. Yakovlev, C. O. Heinke, W. C. G. Ho, and D. J. Patnaude, Mon. Not. R. Astron. Soc. **412**, L108 (2011); D. Blaschke, H. Grigorian, D. N. Voskresensky, and F. Weber, Phys. Rev. C **85**, 022802 (2012); A. Sedrakian, Astron. Astrophys. **555**, L10 (2013).

[3] G. Baym, C. J. Pethick, D. Pines, and M. Ruderman, Nature (London) **224**, 872 (1969).

[4] P. W. Anderson and N. Itoh, Nature (London) **256**, 25 (1975).

[5] N. Andersson, K. Glampedakis, W. C. G. Ho, and C. M. Espinoza, Phys. Rev. Lett. **109**, 241103 (2012).

[6] N. Chamel, Phys. Rev. Lett. **110**, 011101 (2013).

[7] R. Prix, G. L. Comer, and N. Andersson, Astron. Astrophys. **381**, 178 (2002).

[8] N. Andersson and G. L. Comer, Living Rev. Relativity **10**, 1 (2007).

[9] N. Chamel, Mon. Not. R. Astron. Soc. **388**, 737 (2008).

[10] N. Andersson, G. L. Comer, and D. Langlois, Phys. Rev. D **66**, 104002 (2002).

[11] N. Andersson and G. L. Comer, Mon. Not. R. Astron. Soc. **328**, 1129 (2001).

[12] N. Andersson, G. L. Comer, and R. Prix, Phys. Rev. Lett. **90**, 091101 (2003).

[13] H. Sotani, K. Nakazato, K. Iida, and K. Oyamatsu, Mon. Not. R. Astron. Soc. **428**, L21 (2013).

[14] M. Borumand, R. Joynt, and W. Klúzniak, Phys. Rev. C **54**, 2745 (1996).

[15] N. Chamel and P. Haensel, Phys. Rev. C **73**, 045802 (2006).

[16] M. E. Gusakov and P. Haensel, Nucl. Phys. **A761**, 333 (2005).

[17] M. E. Gusakov, E. M. Kantor, and P. Haensel, Phys. Rev. C **79**, 055896 (2009).

[18] G. Comer and R. Joynt, Phys. Rev. D **68**, 023002 (2003).

[19] G. Comer, Phys. Rev. D **69**, 123009 (2004).

[20] N. Andersson and G L. Comer, Classical Quantum Gravity **18**, 969 (2001).

[21] G. L. Comer, Found. Phys. **32**, 1903 (2002).

[22] B. Carter, in *Relativistic Fluid Dynamics*, edited by A. Anile and M. Choquet-Bruhat(Springer, Heidelberg, 1989).

[23] G. L. Comer and D. Langlois, Classical Quantum Gravity **11**, 709 (1994).

[24] B. Carter and D. Langlois, Phys. Rev. D **51**, 5855 (1995).

[25] B. Carter and D. Langlois, Nucl. Phys. **B531**, 478 (1998).

[26] D. Langlois, A. Sedrakian, and B. Carter, Mon. Not. R. Astron. Soc. **297**, 1189 (1998).

[27] G. Comer, D. Langlois, and L. M. Lin, Phys. Rev. D **60**, 104025 (1999).

[28] R. Prix and M. Rieutord, Astron. Astrophys. **393**, 949 (2002).

[29] N. K. Glendenning, *Compact Stars* (Springer-Verlag, New York, 1997).

[30] J. Boguta and A. R. Bodmer, Nucl. Phys. **A292**, 413 (1977).

[31] A. F. Andreev and E. P. Bashkin, Zh. Eksp. Teor. Fiz. **69**, 319 (1975) [Sov. Phys. JETP **42**, 164 (1976)].

[32] G. A. Lalazissis, J. König, and P. Ring, Phys. Rev. C **55**, 540 (1997).

[33] F. J. Fattoyev, C. J. Horowitz, J. Piekarewicz, and G. Shen, Phys. Rev. C **82**, 055803 (2010).

[34] J. Antoniadis *et al.*, Science **340**, 1233232 (2013).

[35] M. E. Gusakov, E. M. Kantor, and P. Haensel, Phys. Rev. C **80**, 015803 (2009).